1 - Aerodynamics And Flight Simulation

1.1 - HELEN-VESNA Aerodynamic Transition

A large segment of the booster is being reused for its flight-proven status, from the HELEN launch in 2018, detailed in Figure 1. As this includes the motor housing and fin assemblies, the primary component that needs to be re-designed is the avionics bay and payload fairing and therefore the principal aerodynamic investigations centered around payload fairing design, in order to optimize its geometry to provide greater stability without compromising severely on apogee.

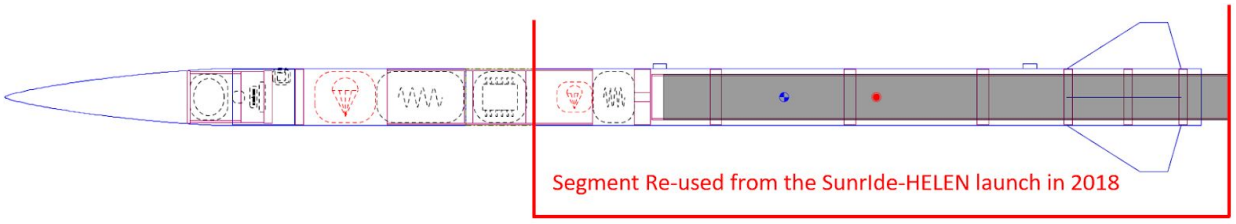

Figure 1: Re-used components from HELEN

Multiple nose cone designs were studied, and initially based on a theoretical design built around shockwave theory, designed for the shortest nose cone length that avoids shock separation, which was then checked against CFD of various nose cone designs at max apogee, conducted using ANSYS's FLUENT module. The angles based on mach number were taken from the shockwave table shown in Figure 2, based on the maximum velocity the rocket would reach from Open rocket data, Mach 1.6-1.7 depending on nose cone shape.

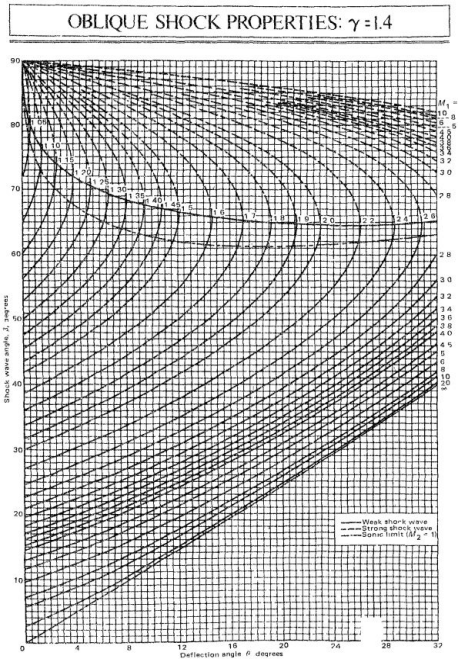

Oblique Shock table [2], showing shock attachment angles vs Mach Number

The base design started with a conical nose cone that transitions into the rocket body, which is designed to minimize flow separation at supersonic speeds around the nose cone profile, shown in Figure 3.

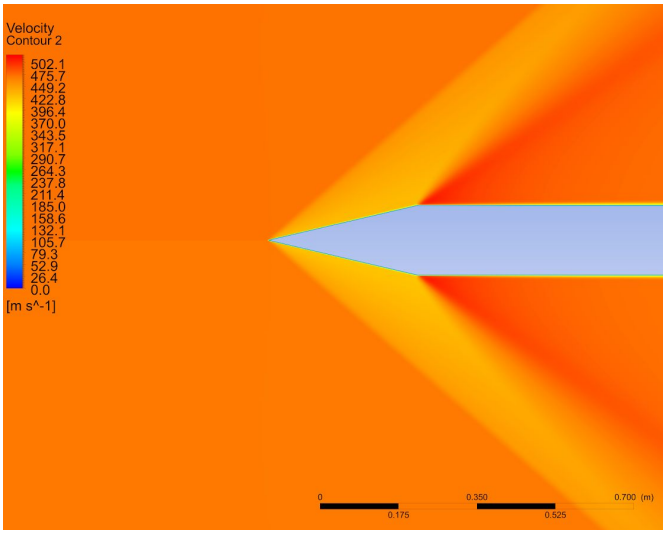

Figure 3: Velocity contours around a conical nose profile, showing shockwaves being generated

The primary drawback of this type of nose cone head is that it has an abrupt transition from its conical profile to the cylindrical shape of the remainder of the nose cone, and that change generates a Prandtl-Meyer expansion wave, as evidenced in Figure 2 by the sudden increase in velocity seen at the junction of the conical nose cone head and the rest of the nose cone.

This effect generates a significant amount of drag and therefore steps were taken to try and reduce the severity of the shockwave being generated.

In order to overcome this, Ogival nose cone designs were studied, which are designed to blend into the cylindrical body and therefore minimize the effects of any shockwaves after the forward tip of the nose cone.

Figure 4 shows an early attempt, using a short and blunt ogival design to maximize stability:

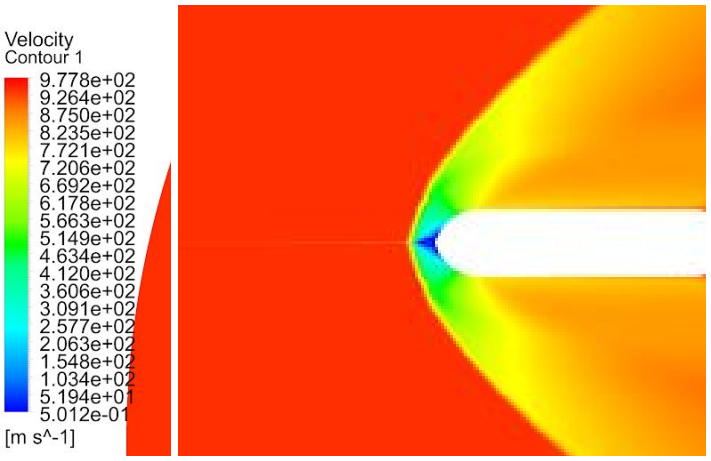

Figure 4: Velocity contours around a blunt ogival nose, image cropped to show area of interest: shockwaves around forward edge of nose cone.

The type of shock generated forward of the nose cone in this instance is called a bow shock, a detached form of the shock seen forward of the conical nose, and generated much more severe drag effects, which can be glimpsed in Figure 3 by observing the rapid and enormous decrease in velocity after the shock, going from around 978 m/s to ~515m/s after the shock.

One positive sign that can be noticed is at the transition region between the forward Ogive shape and the remainder of the cylindrical segment of the nose cone, the expansion wave generated is much less severe, and demonstrates the validity of the theoretical expectation in this instance.

The final nose cone design was therefore created as a compromise maximizing the strengths of all the features outlined above: A long ogival nose cone, designed to maximize stability and altitude whilst minimizing the severity of shocks generated in front of the nose cone and before it. Thereby, the solution maintains the strengths of both conical and ogival designs without sacrificing significantly in other areas. The design is shown in Figure 5:

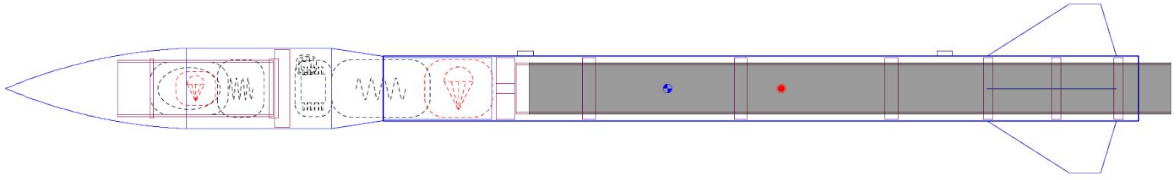

Figure 5: Finalized VESNA Nose Cone design - Ogive with a shape parameter of 0.9.

Though other nose cone designs, such as the Haack series, which are specifically designed to minimize drag, in this situation they present too much of a compromise, either severely reducing stability or apogee based on Open Rocket data.

1.2 - Drag Analysis

Drag values affect the analysis of most segments of the rocket's flight, and therefore we decided to perform CFD studies to determine more accurate values for drag as we have learned from the SunrIde's 2017 and 2018 launches that Open Rocket's default drag values are unreliable.

In order to accomplish this, we setup a 2-Dimensional simulation, using ANSYS Fluent, containing ~350,000 cells and using the K-Omega SST model due to its reliability in such studies.

The CFD studies were initiated in a 2D environment considering the computing resources and time required for multiple analyses at different Mach numbers, alongside the need to run the simulations for 8000 iterations depending on the Mach number.

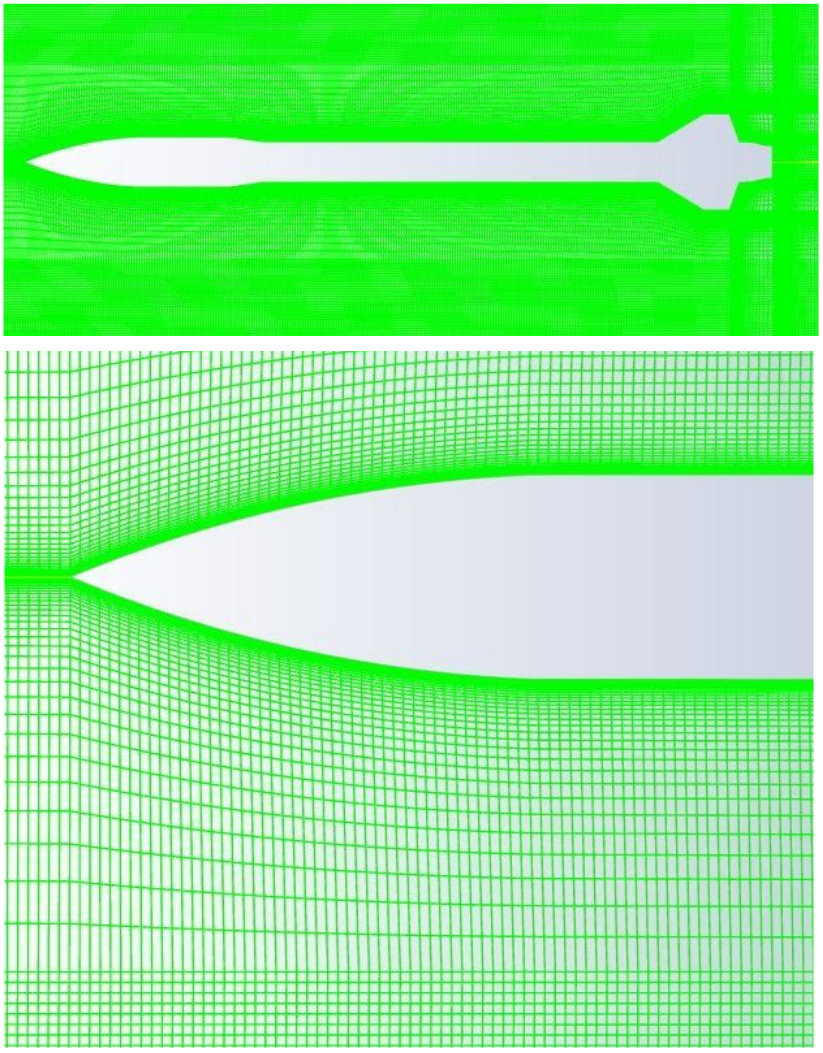

Figure 6: 2D Structured Mesh, Showing rocket body and section view around nose cone to pick up boundary layer characteristics

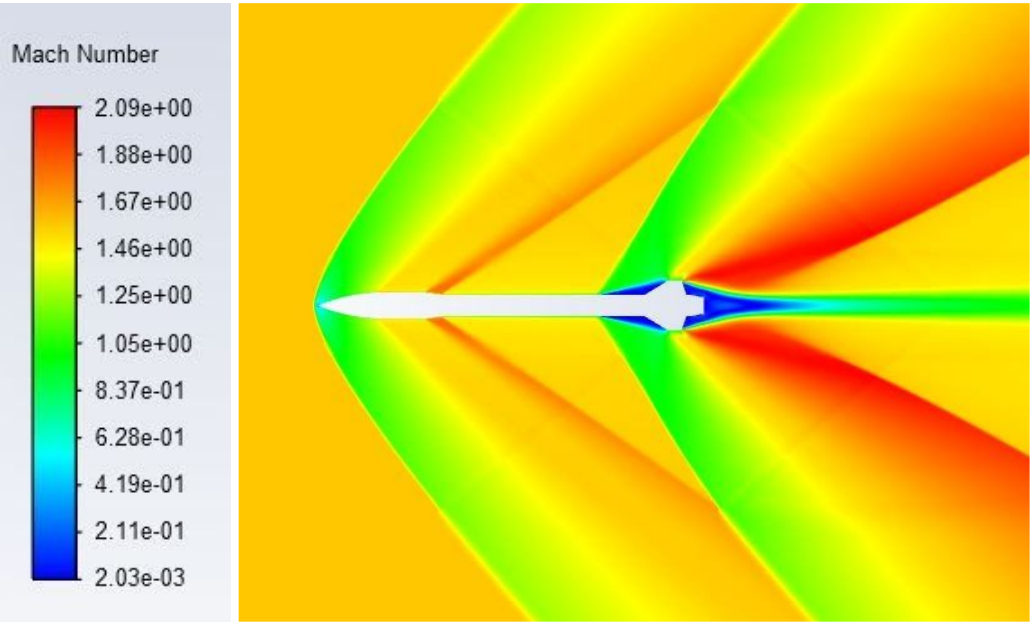

Figure 7: Contours of Mach Number for Rocket Velocity of Mach 1.68

Figures 7 and 8 show CFD results at Mach 1.68, which is slightly higher than the max velocity predicted by Open Rocket. Both contours Perfectly match expectations, keeping in line the understanding established in the earlier section about nose cone design.

An Attached shock is maintained around the nose cone, the severity of velocity decrease is reduced as compared to a blunt Ogive nose cone design, therefore satisfying the design requirements we set out to meet.

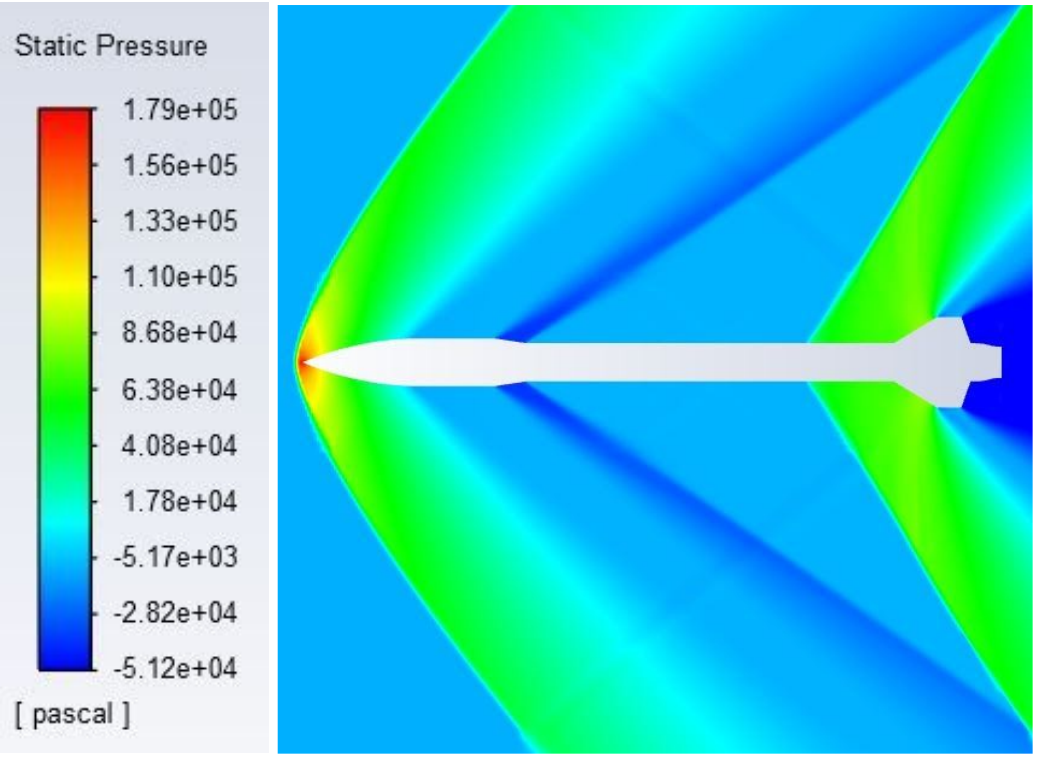

Figure 8: Contours of Static Pressure for Rocket Velocity of Mach 1.68

The results of the simulation are tabulated in Table 1, showing Mach number against Drag Coefficient. These values were inserted into Open Rocket using the CD Override Plugin, and used to plot the graphs in the next section, to visualize rocket trajectory and behaviour. The plot of Mach vs Drag Coefficient can be seen in Figure 9.

Mach	Drag Co.	Mach	Drag Co.
0.66	0.1073	1.01	0.1724
0.71	0.1160	1.02	0.1821
0.81	0.1311	1.04	0.1939
0.86	0.1523	1.06	0.1993
0.91	0.1566	1.20	0.2044
0.94	0.1616	1.30	0.1984
0.95	0.1645	1.40	0.1628
0.97	0.1693	1.50	0.1552
0.99	0.1709	1.60	0.1445
1.00	0.1707	1.68	0.1592
		1.78	0.1340

Table 1: Mach Numbers with their corresponding Drag Coefficient Values

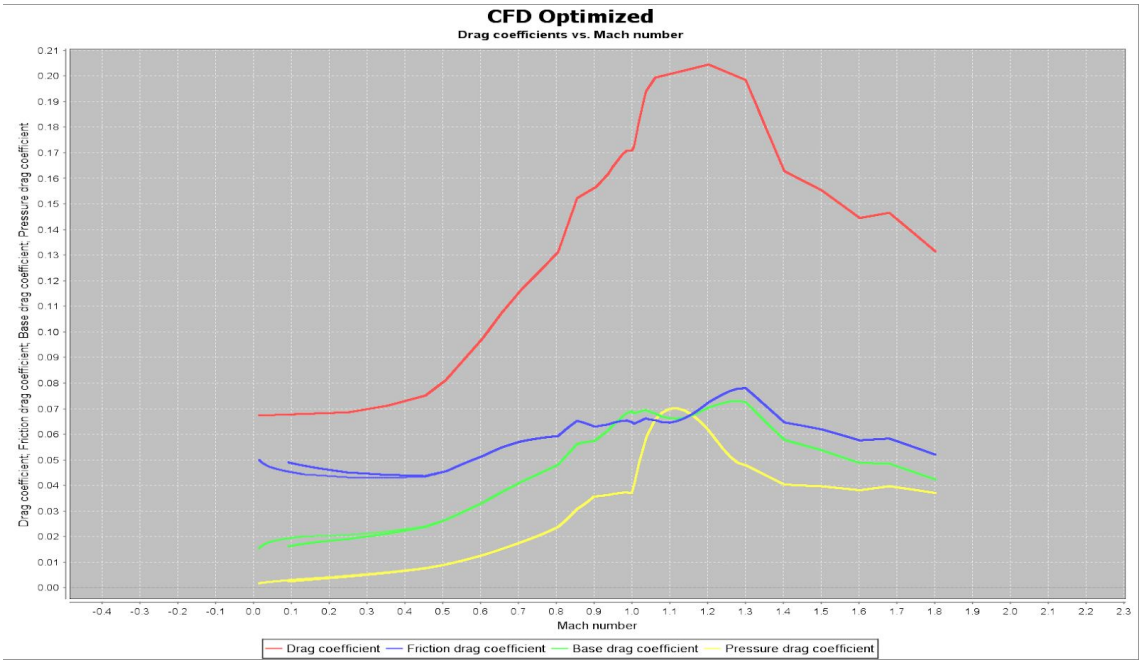

Figure 9: Plot of Drag Coefficients vs Mach Number for VESNA

One of the curves in Figure 9, drag coefficient is a visualization of the data obtained via CFD, the other 3 curves are calculated by Open Rocket based on the CD values. The other plots behave roughly as expected, with the pressure drag plot showing most deviation from expected as the drag due to stronger shockwaves at higher supersonic speeds are not appropriately captured.

Figure 10 shows an Apogee of 41847ft (12755m), this value will likely be lower due to the aforementioned lower pressure drag values at higher mach numbers

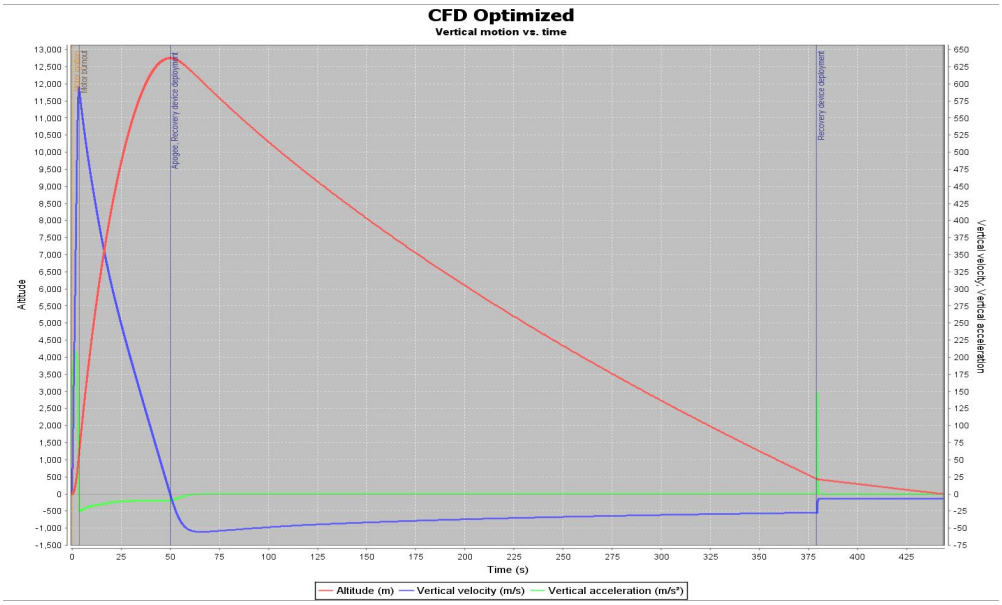

Figure 10: Vertical Motion vs Time for VESNA

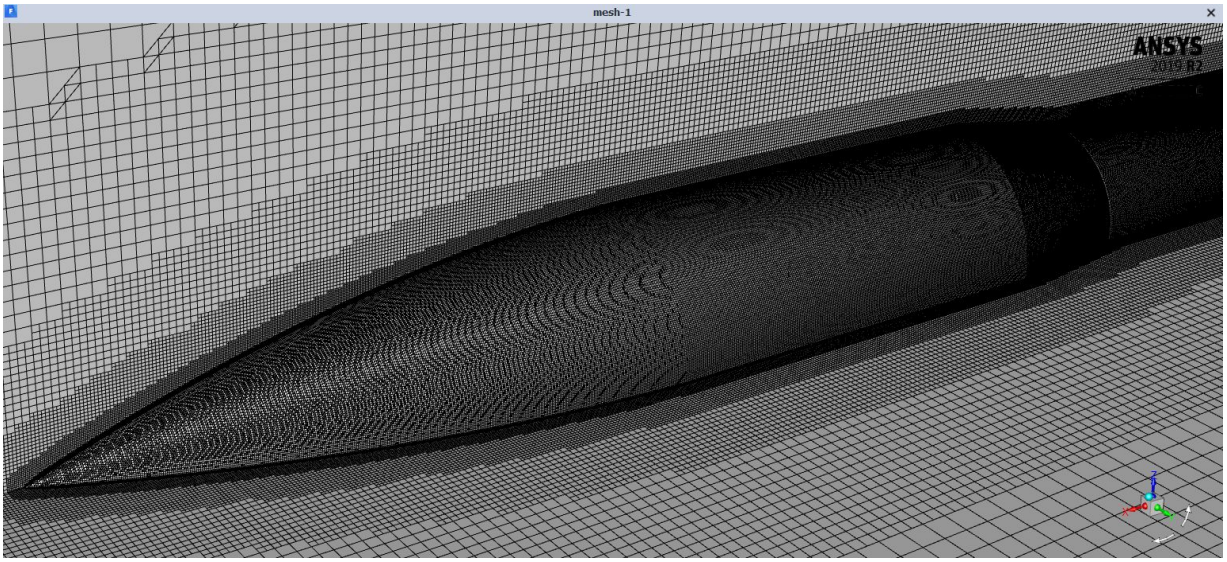

Figure 11: Image of 3D Mesh around Nose Cone for VESNA geometry

Efforts are underway to carry out 3D simulations, we are starting with a basic 3D structured mesh seen in Figure 11. The initial results look promising and this method would yield much more accurate drag calculations.

1.3 - Stability Characteristics

The “Spaceport America Cup Design, Test & Evaluation Guide” [3] lists the following requirements from an Aerodynamic and Stability perspective:

- Flight Stability Margin: 1.5 - 2.0
- Ground Hit Velocity < 9 m/s
- Payload Mass: at least 8.8 lb
- Reach an Apogee of 30,000 ft.

Based on the Openrocket Data with Drag values from CFD, we obtain:

- Flight Stability Margin: 1.51
- Ground Hit Velocity: 6.7 m/s
- Payload Mass: 13.2 lbs
- Apogee: 41,800 ft.

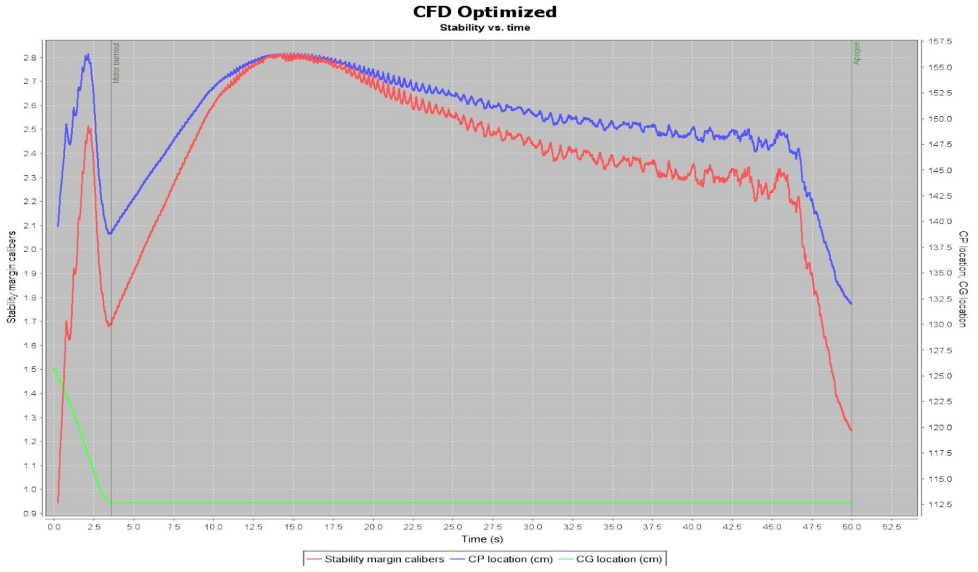

Figure 12: VESNA’s Stability curves vs Time

Figure 12 shows the stability variance with time, the Stability margin caliber values between Ignition and Apogee are higher than SunrIde’s 2018 launch predictions, and we are therefore satisfied with the performance predictions in this regard.

A similar understanding is reached with Figure 13, which shows a smaller roll rate compared to the 2018 HELEN rocket, with the overall trends remaining the same.

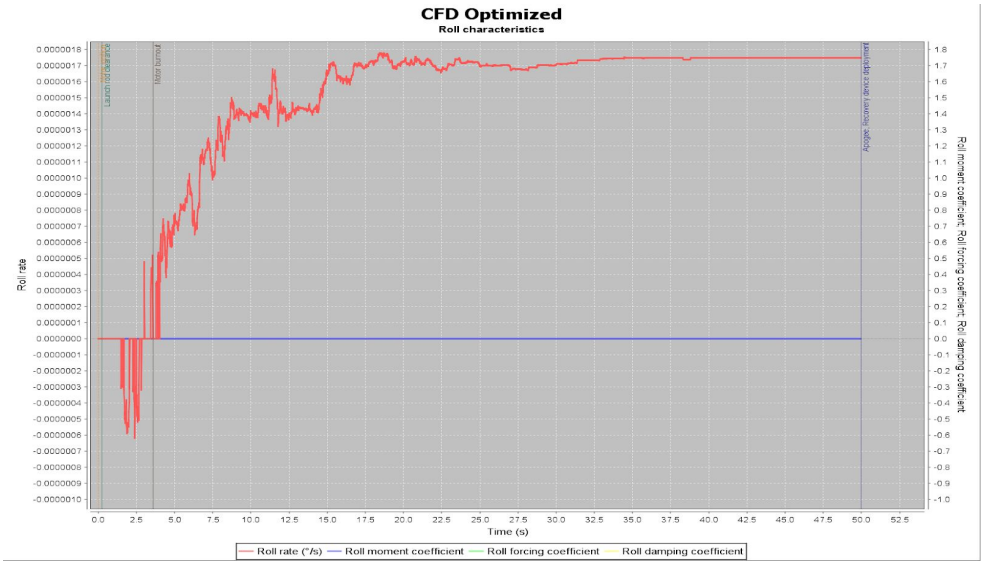

Figure 13: VESNA roll characteristics

References

[1] http://aero-comlab.stanford.edu/Papers/palaniappan.aiaa.04-5383.pdf

[2] Modern Compressible Flow With Historical Perspective, John Anderson

[3]http://www.soundingrocket.org/uploads/9/0/6/4/9064598/sa_cup_irec-design_test___evaluation_guide_20191118__rev_c_final_.pdf

Payload Fairing and Ejection System

To demonstrate the ability to deploy a cubesat, and as part of team SunrIde's ongoing rocket development programme, a payload fairing and cubesat ejection system are integrated into this rocket. Another project at the University of Sheffield are developing a functional 1.5U cubesat which will be launched and ejected from VESNA.

Firstly, the cubesat deployment system involves a compression spring and a plate which pushes the payload along four guide rails, providing enough force to accelerate the payload and push it out the top of the rocket at apogee. The spring will be held in compression for the duration of the flight until apogee, by either an electrically controlled latch or a non-explosive separation device (such as a Frangibolt). This latch will be released at apogee to allow the spring to extend and push the payload. The rails will be made out of aluminium and will be mounted to the bulkhead below and also held together by a centering ring which is mounted to the inside of the fairing halves.

Before the payload is ejected, the two fairing halves must open. A number of non-explosive separation devices will release the two fairing halves, then two gas struts will push the fairing open via a two bar linkage, rotating about a hinge at the base of each fairing half. The gas struts will be held in compression for the duration of the flight and then be able to extend when the fairing halves are separated by the non-explosive separation device.

Along with the payload, the drogue parachute and shock cord will also be ejected from the top of the rocket, and sit between the payload and spring pusher plate during flight. The shock cord threads through the pusher plate and attaches to the hoop which is mounted onto the bulkhead. As the drogue parachute will deploy through the top of the fairing, the fairing must remain open after deployment. The gas struts used to open the fairing will then keep the fairing open and apply a damping force to reduce vibration of the fairing halves during descent.

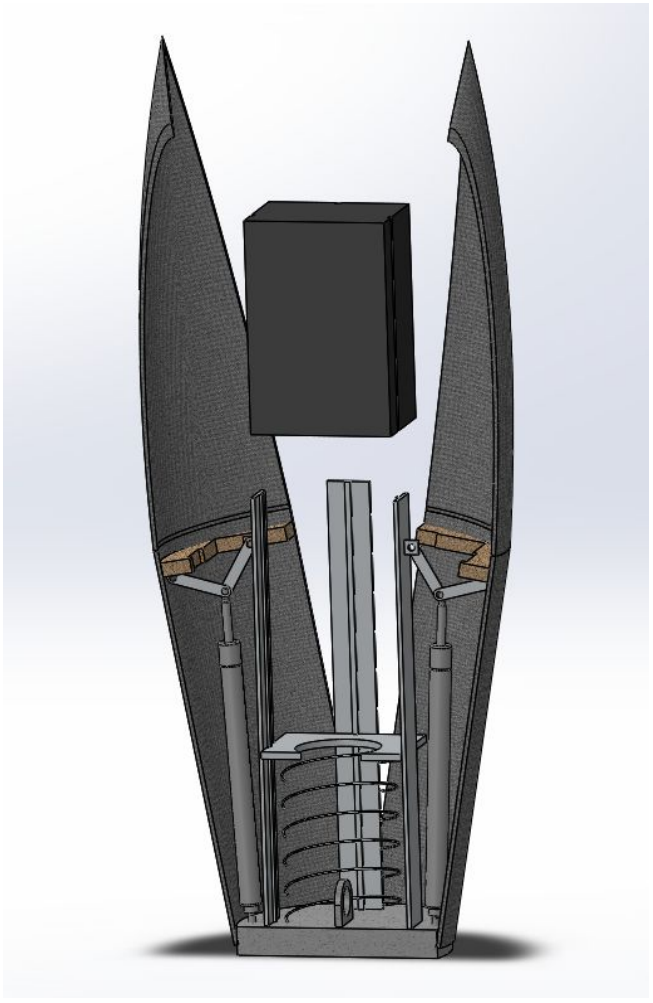

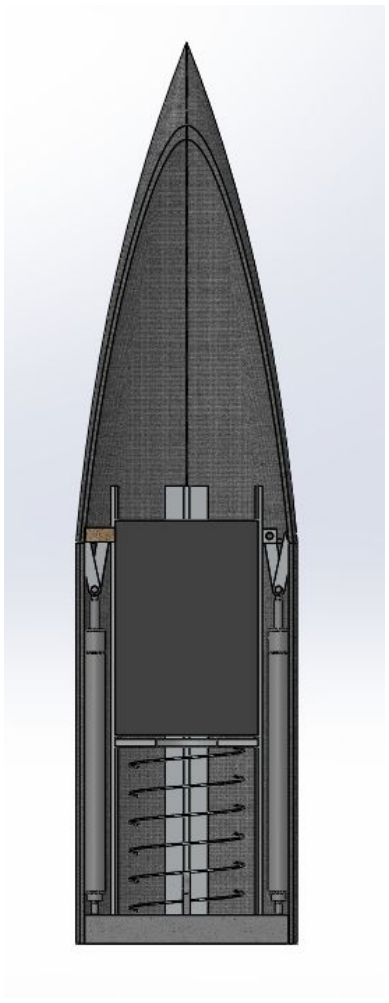

Avionics

1.Teensy 3.6 Microcontroller

The IMU's and sensors will all be connected to a central Teensy 3.6 microcontroller consisting of a 32 bit 180 Mhz ARM Cortex-M4 processor and measuring 60.96 by 17.78 mm. The board contains a total of 62 I/0 pins, 42 of which are breadboard supported and all of which have a maximum voltage application of 3.3V. The Teensy 3.6 has 1024 KB of program flash, 256 KB of FlexNVM and 4 KB of FlexRAM. For each of these data storage spaces, the program flash is non-volatile memory that can execute program code, the FlexNVM is non-volatile memory that can execute program code, store data or back up EEPROM data (Electrically Erasable Programmable Read-Only Memory, he RAM can be used traditionally or as high endurance EEPROM storage and it also accelerates flash programming.

(Figure 5: top side of Teensy 3.6 board https://www.pjrc.com/store/teensy36.html)

For longer term off-processor data storage there is a native (4 bit SDIO) micro SD card port built into one end of the board, allowing for inflight data from all of the connected sensors to be stored and removed from the rocket after a flight so that the data can easily be analysed.

2.Stratologger CF

The PerfectFlite StratologgerCF Altimeter will be used has a backup for the parachute release and storage of the inflight data. It is suitable for the required task due to the fact that it has a built-in voltmeter allowing for the recording of data even after the main power battery has been detached. The data storage capacity is up to 15 flights each a total of 18 minutes at an industry standard sample rate of 20 per second.

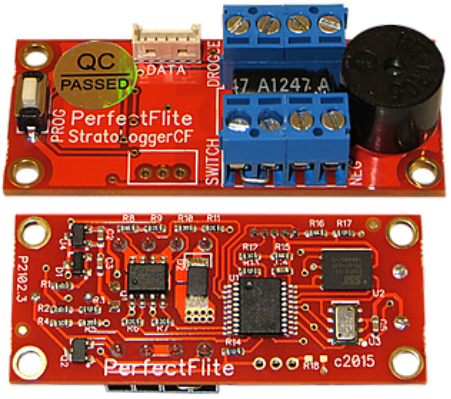

(Figure 6: PerfectFlite Stratologger CF Altimeter http://www.perfectflite.com/SLCF.html)

3.GPS

COTS GPS System: Spot Trace GPS Tracking - COTS

The spot trace GPS tracking device is primarily an anti-theft device, and can be used for the purpose of recovering the rocket, payload fairing and the payload. This device complies with part 15 of FCC rules and limits for a Class B device under FCC rules. The GPS coordinates can be found using the Spot Trace's online subscription plan. The coordinates will be displayed on the Spot Trace's website has a minimum refresh rate of 2.5 minutes. The battery will last a minimum of 15 days with the 2.5 minutes refresh rate. This device was used in our previous rocket part in the Spaceport America Cup and was found to be reliable when recovering the rocket.

Three Spot Trace GPS devices will be used: The avionics bay (attached to the bottom part of the rocket), the payload and the payload fairing each will have a Spot Trace attached to it. The GPS system will be mounted in the rocket body which has least electromagnetic

radiation from the avionic systems and where the radio frequencies are not obstructed by carbon fibre composite materials.

* Transmit Frequencies: 1611.25 Mhz - 1618.75 Mhz (4 Channels)

* Max Power Out: 24.66 dBm EIRP

SRAD Flight Computer GPS:

The GPS used for the SRAD flight computer will be the Ublox NEO/LEA-M8T series GPS. These GPS can receive GPS, GLONASS and GALILEO satellite systems, this will allow for a maximum number of satellite signals received. I²C serial protocol will be used to interface with the Teensy microcontroller. This GPS can receive a satellite RF signal upto 100,000ft and has been used in cube-sats in the past.

This GPS is primarily used to retrieve live GPS data of the flight trajectory which can then be used to determine the feasibility of using this GPS system for future launches.

4.Data Transmission

SRAD Flight Computer Telemetry:

The SRAD computer telemetry will use RF-LoRa for telemetry link. This has a range of 16km LOS and utilizes a *915Mhz frequency range* with less than *100mw* signal strength. The ground station will have a LoRa receiver with a Yagi Antenna to receive telemetry from the rocket. A patch antenna will be used on board the rocket for the SRAD Flight Computer LoRa Telemetry link. I²C serial protocol will be used to interface with the Teensy microcontroller.

5.Power Supplies

The material a battery is made from is an important consideration as this decision could lead to a more efficient, safer and lighter overall system. The properties of different battery types can be found in Figure

	NiCd	NiMH	Lead Acid	Li-ion	Li-ion polymer	Reusable Alkaline
Gravimetric Energy Density (Wh/kg)	45-80	60-120	30-50	110-160	100-130	80 (initial)
Internal Resistance (includes peripheral circuits) in mΩ	100 to 200[1] 6V pack	200 to 300[1] 6V pack	<100[1] 12V pack	150 to 250[1] 7.2V pack	200 to 300[1] 7.2V pack	200 to 2000[1] 6V pack
Cycle Life (to 80% of initial capacity)	1500[2]	300 to 500[2,3]	200 to 300[2]	500 to 1000[3]	300 to 500	50[3] (to 50%)
Fast Charge Time	1h typical	2-4h	8-16h	2-4h	2-4h	2-3h
Overcharge Tolerance	moderate	low	high	very low	low	moderate
Self-discharge / Month (room temperature)	20%[4]	30%[4]	5%	10%[5]	~10%[5]	0.3%
Cell Voltage (nominal)	1.25V[6]	1.25V[6]	2V	3.6V	3.6V	1.5V
Load Current - peak - best result	20C 1C	5C 0.5C or lower	5C[7] 0.2C	>2C 1C or lower	>2C 1C or lower	0.5C 0.2C or lower
Operating Temperature (discharge only)	-40 to 60°C	-20 to 60°C	-20 to 60°C	-20 to 60°C	0 to 60°C	0 to 65°C
Maintenance Requirement	30 to 60 days	60 to 90 days	3 to 6 months[9]	not req.	not req.	not req.
Typical Battery Cost (US$, reference only)	$50 (7.2V)	$60 (7.2V)	$25 (6V)	$100 (7.2V)	$100 (7.2V)	$5 (9V)
Cost per Cycle (US$)[11]	$0.04	$0.12	$0.10	$0.14	$0.29	$0.10-0.50
Commercial use since	1950	1990	1970 (sealed lead acid)	1991	1999	1992

(Figure 2, https://batteryuniversity.com/learn/archive/whats_the_best_battery, shows the different properties of typical battery types)

As VESNA will likely experience both high and low temperature during its flight due to the ascent speed, place of launch and altitude it reaches it would be desirable to have an operating temperature that extends below 0 °C and a reasonable maximum operating temperature. Another important property to look at was the maintenance requirements of the battery, as this could cause the battery to fail if it is not maintained properly; limiting the time frame we can hold onto the batteries, potentially raising the cost of the project. The deciding factor however was the energy density of the battery type as this directly translates to the mass of the avionics system which should ideally be minimal.

Selected Battery type

Due to the properties of the Li-ion battery it has been selected as the ideal battery type to use for VESNA, this comes as a result of the battery having a reasonable operating temperature range that extends below 0 °C ; no maintenance requirements and importantly high energy density.While the battery has a major disadvantage in its overcharging tolerance this is an issue that can be managed during the testing stage and will never be encountered during the flight.

(source:
https://www.robotshop.com/community/tutorials/show/basics-how-do-i-choose-a-battery)

6.Power management

The voltage of the power supply will depend on voltage and power requirements of components. As many of the components will have different voltage requirements this source will need to be managed. There are different approaches that can be used.

Multiple supplies:

- Less time taken to integrate into the system.
- Potentially more energy efficient.
- More potential points of failure. If one supply fails an important. subsystem might be compromised.
- Safer for components with a large difference of operating voltage.
- Relatively heavy.

Single supply:

- Reduces overall mass.
- More time needed to integrate into the system.
- Easier to manage and troubleshoot any problems.
- Single point of failure, if this supply fails the whole system is compromised.
- Will need Voltage management and measures to supply the correct voltage.
- Potentially unsafe with a large range of voltage requirements.

Both methods of voltage management provide major advantages and disadvantages;due to this a decision was made to use a mixture of these voltage management systems. Due to the potential danger of using a single high voltage power supply to power the entire avionics bay; the system will be powered by a set of different size batteries. High voltage components will be powered by a separate power supply to the rest of the avionics bay. However to reduce the overall mass of the avionics bay the different power supplies will use their own voltage management to power all of the components with a similar voltage requirement.